SIAM J. SCI. COMPUT.
Vol. 28, No. 6, pp. 2054–2074

AN EMBEDDED BOUNDARY METHOD FOR THE WAVE EQUATION WITH DISCONTINUOUS COEFFICIENTS*

HEINZ-OTTO KREISS† AND N. ANDERS PETERSSON‡

Abstract. A second order accurate embedded boundary method for the two-dimensional wave equation with discontinuous wave propagation speed is described. The wave equation is discretized on a Cartesian grid with constant grid size and the interface (across which the wave speed is discontinuous) is allowed to intersect the mesh in an arbitrary fashion. By using ghost points on either side of the interface, previous embedded boundary techniques for the Neumann and Dirichlet problems are generalized to satisfy the jump conditions across the interface to second order accuracy. The resulting discretization of the jump conditions has the desirable property that each ghost point can be updated independently of all other ghost points, resulting in a fully explicit time-integration method. We prove that the one-dimensional restriction of the method is stable without damping for arbitrary locations of the interface relative to the grid. For the two-dimensional case, the previously developed fourth order A^TA-dissipation is generalized to handle jump conditions. We demonstrate that this operator provides sufficient stabilization to enable long-time simulations while being weak enough to preserve the accuracy of the solution. Numerical examples are given where the method is used to study electromagnetic scattering of a plane wave by a dielectric cylinder. The numerical solutions are evaluated against the analytical solution due to Mie, and pointwise second order accuracy is confirmed.

Key words. wave equation, discontinuous coefficients, jump condition, embedded boundary, finite differences

AMS subject classifications. 65M06, 65M12

DOI. 10.1137/050641399

1. Introduction.

This paper describes a second order accurate Cartesian embedded boundary method for the two-dimensional wave equation with discontinuous wave propagation speed. Motivated by wave propagation problems from applications like seismology, acoustics, and general relativity, where the underlying differential equations are systems of second order hyperbolic partial differential equations, we develop a numerical method that directly discretizes the wave equation in second order formulation. This approach extends previous research [1, 2, 3] to the case of discontinuous coefficients.

For every second order hyperbolic system, there is an equivalent but larger first order system. For example, two-dimensional acoustic wave propagation is governed by a scalar second order wave equation for the pressure, or by a system of three first order hyperbolic equations governing the two velocity components and the pressure. Most previous numerical methods for this type of problem have focused on the first order formulation [4, 5, 6]. For linear wave propagation, a staggered grid is often used to avoid complications with stability of extra numerical boundary conditions [7] and spurious waves traveling in the wrong direction [8]. However, Cartesian staggered grid discretizations are difficult to generalize to handle complex geometries, that is, boundaries that intersect the grid in an arbitrary way.

*Received by the editors September 28, 2005; accepted for publication (in revised form) May 24, 2006; published electronically December 5, 2006. This work was performed under the auspices of the U.S. Department of Energy by the University of California, Lawrence Livermore National Laboratory, under contract W-7405-Eng-48.

http://www.siam.org/journals/sisc/28-6/64139.html

†Träskö-Storö Institute of Mathematics, Stockholm, Sweden (hokreiss@nada.kth.se).

‡Center for Applied Scientific Computing, LLNL, Livermore, CA (andersp@llnl.gov).

The accuracy of a finite difference approximation of the wave equation with discontinuous coefficients was analyzed by Brown [9]. For the one-dimensional case, he proved that the amplitude error in reflected and transmitted waves is determined by the accuracy by which the jump conditions are discretized, while the phase error is determined by the accuracy of the discretization in the interior of the domain. In the one-dimensional case, Tikhonov and Samarskiĭ's [10] averaging formula was used to obtain a second order accurate approximation without explicitly discretizing the jump conditions. Numerical calculations indicated a significant benefit of combining the second order treatment of the jump conditions with a fourth order method in the interior of the domain. Unfortunately, it is not known how to generalize the averaging formula to the two-dimensional case when the discontinuity is not aligned with the grid, and the combinations of a first order treatment of the jump conditions with a second or fourth order formula away from the interface gave less impressive results than in the one-dimensional case.

A fully second order immersed interface method for solving the two-dimensional acoustic wave equation with discontinuous coefficients was developed by Zhang and LeVeque [11]. Here, the problem was written as a hyperbolic system of three first order equations and special difference formulas were developed near the interface, which take the location of the interface and the jump conditions into account to achieve second order accuracy. For each grid point next to the interface, a linear system with 54 equations for 54 unknowns had to be solved to find the values of the coefficients in the local difference formula. For more complicated hyperbolic systems (such as the elastic wave equation), even larger systems of equations must be solved to set up the coefficients.

Finite difference methods for the time-dependent Maxwell equations have been studied extensively, and a relatively recent overview of the field is provided by Hesthaven [12]. Maxwell's equations are usually written as a first order hyperbolic system and a Cartesian staggered grid is often employed to discretize the equations in space. Several second, fourth, and even higher order accurate schemes have been derived to handle embedded discontinuous coefficients in the one-dimensional case [13, 14, 15, 16], but these methods generalize only to the two-dimensional case when the material interface is parallel to a grid direction. A brief description of a compact fourth order accurate implicit staggered grid scheme based on Pade' approximations is presented by Turkel and Yefet [17]. Here the Dirichlet condition associated with a perfectly electric conducting boundary is satisfied on an embedded boundary by locally modifying the uniform mesh to make the nearest grid points fall on the boundary. However, it is not clear how this approach can be generalized to handle jump conditions across material interfaces. Furthermore, this approach can result in a severe time step restriction due to small cells at the boundary. An alternative to the staggered grid approach is presented by Cai and Deng [18], who solve the first order hyperbolic system on a node-based grid by combining a Lax–Wendroff scheme in the interior with an upwinding approach for satisfying jump conditions across an embedded material interface. However, solving a first order system on a node-based grid can lead to the aforementioned problem with spurious waves traveling in the wrong direction [8]. Furthermore, the mesh needs to be finer to achieve the same accuracy compared to when the wave equation is solved in second order formulation [1].

Higher order finite difference schemes for Maxwell's equations have also been extended to the curvilinear case [19] and to overlapping grids [20], but these approaches rely on the availability of a smooth mesh conforming to the interface. We also remark that there are many Cartesian embedded boundary methods for elliptic and parabolic

partial differential equations, e.g., [21, 22, 23, 24, 25, 26].

In this paper, we consider the scalar second order wave equation in a two-dimensional domain $\Omega = \Omega_I \cup \Omega_{II}$, with a piecewise constant coefficient $\rho(\boldsymbol{x}) > 0$,

$$\rho(\boldsymbol{x}) = \begin{cases} \rho_I, & \boldsymbol{x} \in \Omega_I, \\ \rho_{II}, & \boldsymbol{x} \in \Omega_{II}. \end{cases}$$

Let $u(\boldsymbol{x}, t)$ and $w(\boldsymbol{x}, t)$ denote the solutions in the subdomains Ω_I and Ω_{II}, satisfying

$$u_{tt} = \frac{1}{\rho_I}\Delta u + F(\boldsymbol{x}, t), \qquad \boldsymbol{x} \in \Omega_I, \quad t \geq 0, \tag{1}$$

$$w_{tt} = \frac{1}{\rho_{II}}\Delta w + F(\boldsymbol{x}, t), \quad \boldsymbol{x} \in \Omega_{II}, \quad t \geq 0, \tag{2}$$

$$u(\boldsymbol{x}, 0) = U_0(\boldsymbol{x}), \quad u_t(\boldsymbol{x}, 0) = U_1(\boldsymbol{x}), \qquad \boldsymbol{x} \in \Omega_I, \tag{3}$$

$$w(\boldsymbol{x}, 0) = W_0(\boldsymbol{x}), \quad w_t(\boldsymbol{x}, 0) = W_1(\boldsymbol{x}), \qquad \boldsymbol{x} \in \Omega_{II}. \tag{4}$$

Here, $F(\boldsymbol{x}, t)$ is a forcing function. Let Γ be the smooth interface between Ω_I and Ω_{II}, across which the solutions are coupled by the jump conditions

$$u = w, \qquad \boldsymbol{x} \in \Gamma, \quad t \geq 0, \tag{5}$$

$$\frac{1}{\rho_I}\frac{\partial u}{\partial n} = -\frac{1}{\rho_{II}}\frac{\partial w}{\partial n}, \quad \boldsymbol{x} \in \Gamma, \quad t \geq 0. \tag{6}$$

Note that the normal derivatives are taken outward from both Ω_I and Ω_{II}. Hence we have the minus sign in the latter equation.

For the purpose of our discussion, we assume that Ω_I is a bounded domain inside Ω_{II}, and that Ω_{II} has a rectangular outer boundary where Dirichlet or Neumann boundary conditions are enforced. The interface between Ω_I and Ω_{II} can however have an arbitrary smooth shape. As will be demonstrated below, the method can be generalized to several subdomains. Nonrectangular outer boundaries can be handled using the embedded boundary techniques in [2] and [3].

We discretize the two-dimensional wave equations on a Cartesian grid $\boldsymbol{x}_{i,j} = (ih, jh)$ in space, where $h > 0$ is the grid size, and let $t_n = n\delta_t$, $n = 0, 1, 2, \ldots$, denote the time-discretization with step size $\delta_t > 0$. We take $u^n_{i,j}$ and $w^n_{i,j}$ to be the difference approximations of $u(x_i, y_j, t_n)$ and $w(x_i, y_j, t_n)$, respectively. At all grid points interior to Ω_I, a second order accurate approximation of the Laplacian of u is given by

$$\Delta_h u^n_{i,j} =: \frac{1}{h^2}(u^n_{i+1,j} + u^n_{i-1,j} + u^n_{i,j+1} + u^n_{i,j-1} - 4u^n_{i,j}), \quad \boldsymbol{x}_{i,j} \in \Omega_I. \tag{7}$$

In order to form (7) at all grid points in Ω_I, we also define $u^n_{i,j}$ at the set of ghost points G_I:

$$G_I = \{(i, j),\ \boldsymbol{x}_{i,j} \notin \Omega_I,\ \text{but at least one of } \boldsymbol{x}_{i\pm1,j} \in \Omega_I \text{ or } \boldsymbol{x}_{i,j\pm1} \in \Omega_I\}.$$

A corresponding formula is used to approximate the Laplacian of w at all interior grid points of Ω_{II} using a corresponding set of ghost points G_{II}.

The solution at the ghost points are determined by the jump conditions (5) and (6). We start by considering the ghost point $u_{i,j}$; see Figure 1.

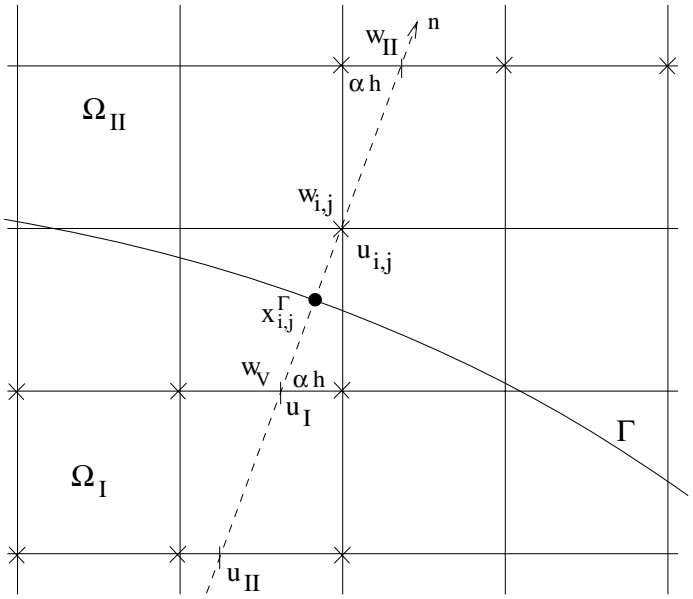

FIG. 1. *The points used for discretizing the jump conditions.*

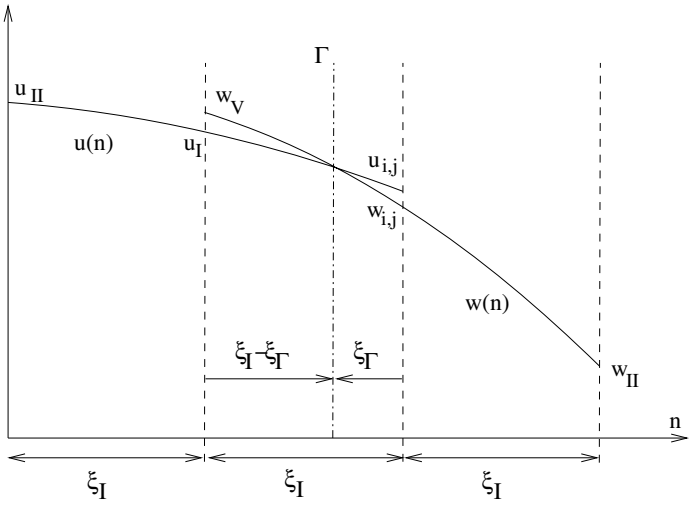

FIG. 2. *The solution along the normal to the interface is continuous, but its first derivative is discontinuous.*

We can derive second order approximations for the value and normal derivative on the boundary using Lagrange interpolation between $u_{i,j}$, u_I, and u_{II} (see Figure 2):

$$B^D_{i,j}u =: g^D_0(\xi_\Gamma)u_{i,j} + g^D_I(\xi_\Gamma)u_I + g^D_{II}(\xi_\Gamma)u_{II} = u(\boldsymbol{x}^\Gamma_{i,j}) + \mathcal{O}(h^2), \qquad (i,j) \in G_I, \tag{8}$$

$$B^N_{i,j}u =: g^N_0(\xi_\Gamma)u_{i,j} + g^N_I(\xi_\Gamma)u_I + g^N_{II}(\xi_\Gamma)u_{II} = \frac{\partial u}{\partial n}(\boldsymbol{x}^\Gamma_{i,j}) + \mathcal{O}(h^2), \quad (i,j) \in G_I. \tag{9}$$

The values u_I and u_{II} are obtained by Lagrange interpolation, in this case, along the

horizontal grid lines y_{j-1} and y_{j-2},

$$u_I^n = r_0 u_{i,j-1}^n + r_1 u_{i-1,j-1}^n + r_2 u_{i-2,j-1}^n, \tag{10}$$

$$u_{II}^n = r_3 u_{i,j-2}^n + r_4 u_{i-1,j-2}^n + r_5 u_{i-2,j-2}^n. \tag{11}$$

The coefficients g^D and g^N are given in section 4.

To derive corresponding formulas for w along the same normal, we introduce the virtual ghost point value w_v, defined at the same location as u_I; see Figure 1. Since w_v is outside Ω_{II} and it is in general located in between grid points, this value is only used to form the discrete jump conditions. Lagrange interpolation between w_v, $w_{i,j}$, and w_{II} (see Figure 2) gives for $(i,j) \in G_I$

$$\begin{aligned} V_{i,j}^D w &=: g_0^D(\xi_I - \xi_\Gamma) w_v + g_I^D(\xi_I - \xi_\Gamma) w_{i,j} + g_{II}^D(\xi_I - \xi_\Gamma) w_{II} \\ &= w(\boldsymbol{x}_{i,j}^\Gamma) + \mathcal{O}(h^2), \end{aligned} \tag{12}$$

$$\begin{aligned} V_{i,j}^N w &=: g_0^N(\xi_I - \xi_\Gamma) w_v + g_I^N(\xi_I - \xi_\Gamma) w_{i,j} + g_{II}^N(\xi_I - \xi_\Gamma) w_{II} \\ &= \frac{\partial w}{\partial n}(\boldsymbol{x}_{i,j}^\Gamma) + \mathcal{O}(h^2). \end{aligned} \tag{13}$$

Note that there is a symmetry between the interpolation formulas for u_I and w_{II} that simplifies the calculation of w_{II}. If the normal going through $\boldsymbol{x}_{i,j}$ intersects the horizontal grid line $y = y_{j-1}$ at $x = x_i - \alpha h$, the extension of the same normal will intersect the grid line $y = y_{j+1}$ at $x = x_i + \alpha h$. The Lagrange interpolation formula for w_{II}^n therefore becomes

$$w_{II}^n = r_0 w_{i,j+1}^n + r_1 w_{i+1,j+1}^n + r_2 w_{i+2,j+1}^n.$$

Inserting the discrete approximations of the value and normal derivatives of u and w into the jump conditions (5), (6) results in the discretized jump conditions

$$B_{i,j}^D u^n = V_{i,j}^D w^n, \tag{14}$$

$$\frac{1}{\rho_I} B_{i,j}^N u^n = -\frac{1}{\rho_{II}} V_{i,j}^N w^n. \tag{15}$$

Hence, we get a 2×2 linear system for the unknowns $(u_{i,j}^n, w_v^n)$:

$$\begin{aligned} &\begin{pmatrix} g_0^D(\xi_\Gamma) & -g_0^D(\xi_I - \xi_\Gamma) \\ g_0^N(\xi_\Gamma)/\rho_I & g_0^N(\xi_I - \xi_\Gamma)/\rho_{II} \end{pmatrix} \begin{pmatrix} u_{i,j}^n \\ w_v^n \end{pmatrix} \\ &= \begin{pmatrix} g_I^D(\xi_I - \xi_\Gamma) w_{i,j}^n + g_{II}^D(\xi_I - \xi_\Gamma) w_{II}^n - g_I^D(\xi_\Gamma) u_I^n - g_{II}^D(\xi_\Gamma) u_{II}^n \\ -(g_I^N(\xi_I - \xi_\Gamma) w_{i,j}^n + g_{II}^N(\xi_I - \xi_\Gamma) w_{II}^n)/\rho_{II} - (g_I^N(\xi_\Gamma) u_I^n + g_{II}^N(\xi_\Gamma) u_{II}^n)/\rho_I \end{pmatrix}. \end{aligned} \tag{16}$$

We solve this system for $u_{i,j}^n$ and ignore the virtual ghost point value w_v^n. A formula for the w-ghost points can be derived in a similar way.

Note that this discretization of the jump conditions has the desirable property that each ghost point can be updated independently of all other ghost points. Hence, there is no coupling along the boundary.

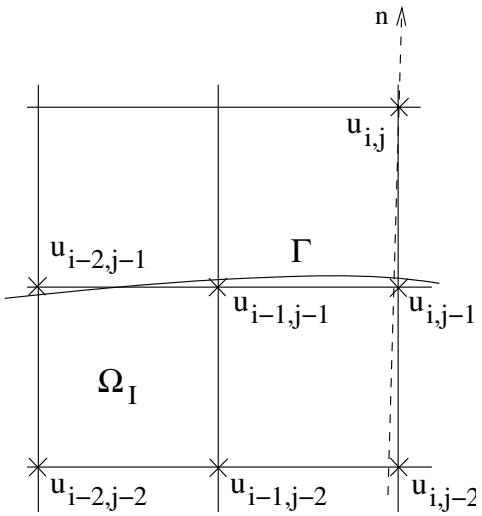

FIG. 3. *The Lagrange interpolation formula for u_I can in rare cases contain outside points.*

Our practical experience with the above interpolation procedure from previous work [2, 3] and the numerical examples in section 6 indicate that it is almost always possible to find enough interior points to compute u_I, u_{II}, and w_{II}, as long as the interface Γ is well resolved on the grid. However, there are rare cases when one or two of the points in the interpolation stencil for u_I can be outside the domain; see Figure 3. In this case, the interface curve has a local maxima just above y_{j-1}, between x_{i-1} and x_i, such that the normal going through $u_{i,j}$ has the form $\boldsymbol{n} = (\zeta, 1-\zeta^2/2)^T$, $\zeta > 0$, $\zeta \ll 1$. Since $\zeta > 0$, we choose to interpolate from $u_{i-2,j-1}$, $u_{i-1,j-1}$, and $u_{i,j-1}$ to obtain u_I. In this situation it is possible for $u_{i-2,j-1}$ to be outside the domain Ω_I, even though the interface is well resolved on the grid. Since the interpolation formula for updating $u_{i,j}$ contains an outside point, we call $u_{i,j}$ a coupled ghost point. However, $u_{i-2,j-1}$ is itself a ghost point which uses only interior points in its interpolation stencils. Such points are called uncoupled ghost points. Hence, if we first compute the uncoupled ghost point value $u_{i-2,j-1}$ we will have all values necessary for computing the coupled ghost point value $u_{i,j}$. In all smooth interface cases we have tried, any coupled ghost points have depended only on uncoupled ghost points, allowing us to use a pointwise procedure where we first update all uncoupled ghost points, followed by updating any coupled ghost points. Some attempts to treat boundaries with corners with the embedded boundary method were reported in [2]. However, the solution can exhibit singularities at the corners which present a more severe set of challenges than merely finding enough grid points to interpolate from. In the following we assume that the interface is smooth and well resolved on the grid.

The remainder of the paper is organized as follows. In section 2, we prove that the discretization of the jump conditions is stable in the one-dimensional case. A simplified stability argument, based on a modified equation model, is presented in section 3. The solvability of the discrete jump conditions in the two-dimensional setting is demonstrated in section 4. Section 5 discusses time-integration and a generalization of the A^TA-dissipation operator (see [2]), which is used to stabilize the scheme for long time-integrations. In section 6, we use the method to study electromagnetic scattering of a plane wave by a dielectric cylinder, where there is a century-old analytical

solution due to Mie [27]. The method is finally applied to two more complicated scattering problems: one including many subdomains and the other with a more irregular interface.

2. Stability. We start by considering the one-dimensional wave equation with discontinuous wave propagation speed,

$$u_{tt} = u_{xx}, \qquad x_{min} \le x \le 0, \quad t \ge 0, \tag{17}$$

$$w_{tt} = c^2 w_{xx}, \quad 0 \le x \le x_{max}, \quad t \ge 0, \tag{18}$$

$$u(x,0) = U_0(x), \quad u_t(x,0) = U_1(x), \qquad x_{min} \le x \le 0, \tag{19}$$

$$w(x,0) = W_0(x), \quad w_t(x,0) = W_1(x), \qquad 0 \le x \le x_{max}, \tag{20}$$

where $c^2 > 0$, $x_{min} < 0$, and $x_{max} > 0$, subject to the Dirichlet boundary conditions

$$u(x_{min}, t) = 0, \quad w(x_{max}, t) = 0, \quad t \ge 0. \tag{21}$$

At the interface, the jump conditions are

$$u(0,t) = w(0,t),$$
$$u_x(0,t) = c^2 w_x(0,t).$$

Using the notation in Figure 4, we discretize the problem in space on a uniform grid $x_\nu = -\alpha h + \nu h$, with grid size $h > 0$, and denote a grid function by $u_\nu(t) = u(x_\nu, t)$. Divided difference operators are defined by $D_+^x u_\nu = (u_{\nu+1} - u_\nu)/h$ and $D_-^x u_\nu = D_+^x u_{\nu-1}$. To model the two-dimensional case, we shift the grid so the discontinuity in the wave speed does not coincide with a grid point, i.e., $0 < \alpha < 1$. We want to focus the discussion on the stability of the discretization of the jump conditions, and we take x_{min} and x_{max} to coincide with grid points, i.e., $x_{min} = x_{-N}$ and $x_{max} = x_N$.

The semidiscrete problem becomes

$$\frac{d^2 u_\nu}{dt^2} = D_+^x D_-^x u_\nu, \qquad \nu = 0, -1, -2, \ldots, -N+1, \tag{22}$$

$$\frac{d^2 w_\nu}{dt^2} = c^2 D_+^x D_-^x w_\nu, \qquad \nu = 1, 2, 3, \ldots, N-1, \tag{23}$$

subject to Dirichlet boundary conditions

$$u_{-N} = 0, \quad w_N = 0, \quad t \ge 0. \tag{24}$$

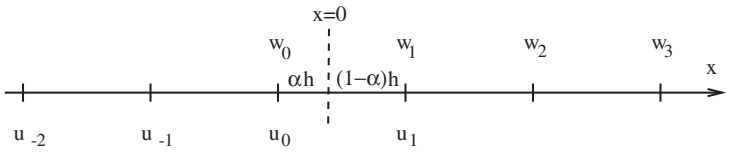

FIG. 4. *Notation for the one-dimensional problem.*

We discretize the jump conditions to second order accuracy by

$$(1-\alpha)u_0 + \alpha u_1 = (1-\alpha)w_0 + \alpha w_1, \tag{25}$$

$$D_+^x u_0 + h\left(\alpha - \frac{1}{2}\right) D_+^x D_-^x u_0 = c^2\left(D_+^x w_0 + h\left(\alpha - \frac{1}{2}\right) D_+^x D_-^x w_1\right). \tag{26}$$

By using (22) and (23), we can write (25), (26) as

$$\alpha u_1 + (\alpha - 1)w_0 = (\alpha - 1)u_0 + \alpha w_1,$$

$$u_1 + c^2 w_0 = u_0 + c^2 w_1 + h^2\left(\alpha - \frac{1}{2}\right)\left(\frac{d^2 w_1}{dt^2} - \frac{d^2 u_0}{dt^2}\right).$$

Solving for w_0 and u_1 yields

$$w_0 = \frac{1}{1-\alpha(1-c^2)}\left(u_0 - \alpha(1-c^2)w_1 + h^2\alpha\left(\alpha - \frac{1}{2}\right)\left(\frac{d^2 w_1}{dt^2} - \frac{d^2 u_0}{dt^2}\right)\right), \tag{27}$$

$$u_1 = \frac{1}{1-\alpha(1-c^2)}\Bigg(c^2 w_1 + (1-\alpha)(1-c^2)u_0 + h^2(1-\alpha)\left(\alpha - \frac{1}{2}\right)\left(\frac{d^2 w_1}{dt^2} - \frac{d^2 u_0}{dt^2}\right)\Bigg). \tag{28}$$

By using (27)–(28) we can eliminate w_0, u_1 from (22)–(23) and obtain

$$b_{11}\frac{d^2 u_0}{dt^2} + b_{12}\frac{d^2 w_1}{dt^2} = \frac{1}{h^2}\left(a_{10}u_{-1} + a_{11}u_0 + a_{12}w_1\right),$$

$$b_{21}\frac{d^2 u_0}{dt^2} + b_{22}\frac{d^2 w_1}{dt^2} = \frac{1}{h^2}\left(a_{21}u_0 + a_{22}w_1 + a_{23}w_2\right).$$

Here,

$$b_{11} = 1 - \alpha(1-c^2) + \left(\alpha - \frac{1}{2}\right)(1-\alpha), \quad b_{12} = -\left(\alpha - \frac{1}{2}\right)(1-\alpha), \tag{29}$$

$$b_{21} = \alpha\left(\alpha - \frac{1}{2}\right), \quad b_{22} = \frac{1}{c^2}\left(1 - \alpha(1-c^2) - c^2\alpha\left(\alpha - \frac{1}{2}\right)\right) \tag{30}$$

and

$$a_{10} = 1 - \alpha(1-c^2), \quad a_{11} = -2 + (1+\alpha)(1-c^2), \quad a_{12} = c^2, \tag{31}$$

$$a_{21} = 1, \quad a_{22} = -2 + \alpha(1-c^2), \quad a_{23} = 1 - \alpha(1-c^2). \tag{32}$$

We can write the semidiscrete problem in matrix form,

$$\begin{pmatrix} 1 & 0 & & & & & & \\ & \ddots & & & & & & \\ & 0 & 1 & 0 & & & & \\ & & 0 & b_{11} & b_{12} & & & \\ & & & b_{21} & b_{22} & 0 & & \\ & & & & 0 & 1/c^2 & 0 & \\ & & & & & & \ddots & \\ & & & & & & 0 & 1/c^2 \end{pmatrix} \frac{d^2}{dt^2} \begin{pmatrix} u_{-N+1} \\ \vdots \\ u_{-1} \\ u_0 \\ w_1 \\ w_2 \\ \vdots \\ w_{N-1} \end{pmatrix}$$

$$= \frac{1}{h^2} \begin{pmatrix} -2 & 1 & & & & & & \\ & \ddots & & & & & & \\ & 1 & -2 & 1 & & & & \\ & & a_{10} & a_{11} & a_{12} & & & \\ & & & a_{21} & a_{22} & a_{23} & & \\ & & & & 1 & -2 & 1 & \\ & & & & & \ddots & & \\ & & & & & 1 & -2 & \end{pmatrix} \begin{pmatrix} u_{-N+1} \\ \vdots \\ u_{-1} \\ u_0 \\ w_1 \\ w_2 \\ \vdots \\ w_{N-1} \end{pmatrix},$$

which we write as

$$\mathcal{B}\mathbf{w}_{tt} = \frac{1}{h^2}\mathcal{A}\mathbf{w}. \tag{33}$$

By (31), (32), the matrix $\mathcal{A}$ is negative diagonally dominant and the off-diagonal elements are positive. Therefore it can be symmetrized by a diagonal scaling $\mathcal{D} > 0$,

$$\tilde{\mathbf{w}} = \begin{pmatrix} \ddots & & & & & & & \\ & d_{-2} & & & & & & \\ & & d_{-1} & & & & 0 & \\ & & & d_0 & & & & \\ & & & & d_1 & & & \\ & 0 & & & & d_2 & & \\ & & & & & & \ddots & \end{pmatrix} \begin{pmatrix} \vdots \\ u_{-2} \\ u_{-1} \\ u_0 \\ w_1 \\ w_2 \\ \vdots \end{pmatrix} =: \mathcal{D}\mathbf{w}, \tag{34}$$

and (33) becomes

$$\tilde{\mathcal{B}}\tilde{\mathbf{w}}_{tt} = \frac{1}{h^2}\tilde{\mathcal{A}}\tilde{\mathbf{w}}, \quad \tilde{\mathcal{B}} = \mathcal{D}\mathcal{B}\mathcal{D}^{-1}, \quad \tilde{\mathcal{A}} = \mathcal{D}\mathcal{A}\mathcal{D}^{-1} = \tilde{\mathcal{A}}^* < 0. \tag{35}$$

Without restriction we can assume that $d_0 = 1$. Then d_1 is determined by the condition that

$$\begin{pmatrix} 1 & 0 \\ 0 & d_1 \end{pmatrix} \begin{pmatrix} a_{11} & a_{12} \\ a_{21} & a_{22} \end{pmatrix} \begin{pmatrix} 1 & 0 \\ 0 & d_1^{-1} \end{pmatrix} = \begin{pmatrix} a_{11} & d_1^{-1}a_{12} \\ d_1 a_{21} & a_{22} \end{pmatrix}$$

is symmetric. By (31), (32), $d_1 = \sqrt{a_{12}/a_{21}} = c$. The corresponding 2×2 submatrix of $\mathcal{B}$ becomes

$$\tilde{\mathcal{B}}_1 = \begin{pmatrix} 1 & 0 \\ 0 & d_1 \end{pmatrix} \begin{pmatrix} b_{11} & b_{12} \\ b_{21} & b_{22} \end{pmatrix} \begin{pmatrix} 1 & 0 \\ 0 & d_1^{-1} \end{pmatrix} = \begin{pmatrix} b_{11} & b_{12}/c \\ cb_{21} & b_{22} \end{pmatrix}.$$

We want to show that

$$\frac{1}{2}(\tilde{\mathcal{B}} + \tilde{\mathcal{B}}^*) > 0, \quad \tilde{\mathcal{B}} = \mathcal{D}\mathcal{B}\mathcal{D}^{-1}. \tag{36}$$

We need to prove this only for $\tilde{\mathcal{B}}_1$, since the remaining part of $\tilde{\mathcal{B}}$ is identical to $\mathcal{B}$, i.e., diagonal with positive elements. By (29), (30),

$$b_{11} = (1-\alpha)\left(\frac{1}{2} + \alpha\right) + \alpha c^2 > 0, \tag{37}$$

$$b_{22} = \frac{1}{c^2}\left(1 - \alpha + \alpha c^2 \left(\frac{3}{2} - \alpha\right)\right) > 0. \tag{38}$$

The characteristic equation, $\det(\frac{1}{2}(\tilde{\mathcal{B}}_1 + \tilde{\mathcal{B}}_1^*) - \mu I) = 0$, is

$$\mu^2 - \mu(b_{11} + b_{22}) + b_{11}b_{22} - \frac{1}{4}\left(\frac{b_{12}}{c} + cb_{21}\right)^2 = 0,$$

with discriminant

$$\Delta = (b_{11} + b_{22})^2 - 4\left(b_{11}b_{22} - \frac{1}{4}\left(\frac{b_{12}}{c} + cb_{21}\right)^2\right) = (b_{11} - b_{22})^2 + \left(\frac{b_{12}}{c} + cb_{21}\right)^2 > 0.$$

The roots are

$$\mu_{1,2} = \frac{1}{2}\left(b_{11} + b_{22} \pm \sqrt{\Delta}\right).$$

Since $b_{11} + b_{22} > 0$ and $\Delta > 0$, both roots are real and positive if $(b_{11} + b_{22})^2 > \Delta$. We have

$$\frac{1}{4}\left((b_{11} + b_{22})^2 - \Delta\right) = b_{11}b_{22} - \frac{1}{4}\left(\frac{b_{12}}{c} + cb_{21}\right)^2$$

$$= \frac{1}{c^2}\left((1-\alpha)\left(\frac{1}{2} + \alpha\right) + \alpha c^2\right)\left(1 - \alpha + \alpha c^2\left(\frac{3}{2} - \alpha\right)\right) - \frac{\left(\alpha - \frac{1}{2}\right)^2}{4}(1 - \alpha - \alpha c^2)^2$$

$$= \frac{1}{c^2}\left((1-\alpha)^2\left(\frac{1}{2} + \alpha\right) - \frac{(\alpha - \frac{1}{2})^2}{4}(1-\alpha)^2\right) > 0.$$

Thus $\frac{1}{2}(\tilde{\mathcal{B}} + \tilde{\mathcal{B}}^*)$ is positive definite.

If $\alpha = \frac{1}{2}$, then, by (29)–(30), $b_{12} = b_{21} = 0$ and $\tilde{\mathcal{B}} = \tilde{\mathcal{B}}^* > 0$. Since $\tilde{\mathcal{A}} = \tilde{\mathcal{A}}^* < 0$, there is an energy estimate and the method is stable.

If $\alpha \neq \frac{1}{2}$, then we make an eigenvector expansion. $\tilde{\mathbf{w}} = e^{\lambda t}\tilde{\mathbf{w}}_0$ is a solution of (35) if $\lambda, \tilde{\mathbf{w}}_0$ are solutions of the eigenvalue problem

$$\left(\lambda^2 \tilde{\mathcal{B}} - \frac{1}{h^2}\tilde{\mathcal{A}}\right)\tilde{\mathbf{w}}_0 = 0. \tag{39}$$

If we can prove that the eigenvalues λ^2 are real, distinct, and negative, then there are no growing modes and the approximation is stable.

If λ^2 is real, then $\tilde{\mathbf{w}}_0$ is also real and the symmetry of $\tilde{\mathcal{A}}$ gives us

$$\lambda^2\langle\tilde{\mathbf{w}}_0, \tilde{\mathcal{B}}\tilde{\mathbf{w}}_0\rangle = \frac{\lambda^2}{2}\langle\tilde{\mathbf{w}}_0, (\tilde{\mathcal{B}} + \tilde{\mathcal{B}}^*)\tilde{\mathbf{w}}_0\rangle = \frac{1}{h^2}\langle\tilde{\mathbf{w}}_0, \tilde{\mathcal{A}}\tilde{\mathbf{w}}_0\rangle,$$

where $\langle \mathbf{u}, \mathbf{v}\rangle$ denotes the usual L_2 inner product. Since $\tilde{\mathcal{A}} < 0$ and $\tilde{\mathcal{B}} + \tilde{\mathcal{B}}^* > 0$, it follows that $\lambda^2 < 0$.

We need the following lemma.

LEMMA 1. *Consider a tridiagonal system of equations*

$$\begin{pmatrix} d_1 & e_1 & 0 & \cdots & \cdots & \cdots & 0 \\ l_2 & d_2 & e_2 & 0 & \cdots & \cdots & 0 \\ 0 & l_3 & d_3 & e_3 & 0 & \cdots & 0 \\ \cdots & \cdots & \cdots & \cdots & \cdots & \cdots & \cdots \\ 0 & \cdots & \cdots & \cdots & 0 & l_n & d_n \end{pmatrix} \begin{pmatrix} z_1 \\ \vdots \\ z_n \end{pmatrix} = 0, \tag{40}$$

and assume that $\theta = 0$ is an eigenvalue. If all $e_j \neq 0$ or all $l_j \neq 0$, then θ is a simple eigenvalue (i.e., the invariant subspace has dimension one).

Proof. Assume that all $e_j \neq 0$ and θ is not a simple eigenvalue. Since the invariant subspace corresponding to θ has dimension larger than one, we can construct an eigenvector with $z_1 = 0$. But then $z_2 = z_3 = \cdots = z_n = 0$, which is a contradiction. Correspondingly, if all $l_j \neq 0$, then there is a solution with $z_n = 0$ which again implies that $z_{n-1} = z_{n-2} = \cdots = z_1 = 0$. This proves the lemma. ∎

We shall now prove that the eigenvalues λ^2 of (39) are simple for all $0 < \alpha < 1$. λ^2 is an eigenvalue of (39) if zero is an eigenvalue of the tridiagonal matrix $Q = h^2\lambda^2\tilde{\mathcal{B}} - \tilde{\mathcal{A}}$. The conditions of Lemma 1 are violated if there is some value of α where at least one element on the subdiagonal of Q is zero *and* one element on the superdiagonal of Q is zero. The only off-diagonal elements of $\tilde{\mathcal{B}}$ are $\tilde{b}_{12}$ and $\tilde{b}_{21}$, $\mathcal{D} > 0$, and $a_{10} = a_{23} = (1-\alpha) + \alpha c^2 > 0$ for all $0 \leq \alpha \leq 1$. Hence, Lemma 1 can only be violated if

$$h^2\lambda^2\tilde{b}_{12} - \tilde{a}_{12} = 0 \quad \text{and} \quad h^2\lambda^2\tilde{b}_{21} - \tilde{a}_{21} = 0. \tag{41}$$

By (29), (30), (31), and (32) we can write (41) as

$$-h^2\lambda^2\left(\alpha - \frac{1}{2}\right)(1-\alpha) - c^2 = 0, \quad h^2\lambda^2\alpha\left(\alpha - \frac{1}{2}\right) - 1 = 0,$$

i.e.,

$$\frac{\alpha - 1}{\alpha} = c^2,$$

which is a contradiction because $c^2 > 0$, but the left-hand side is negative for $0 < \alpha < 1$. Thus the eigenvalues λ^2 of (39) are simple. They are also real because they are solutions of the characteristic equation and smooth functions of α. For $\alpha = \frac{1}{2}$ they are real. Therefore they are real for all values of α because they can only become complex at some value $\alpha = \alpha_0$ if there is an eigenvalue which is not simple. This completes the proof of the following theorem.

THEOREM 1. *The eigenvalues λ^2 of* (39) *are real, distinct, and negative. Therefore the semidiscrete problem* (22), (23) *subject to the boundary conditions* (24) *and the jump conditions* (25), (26) *is stable.*

3. The modified equation. Instead of the complete proof of the last section (which is quite complicated), we shall now use modified equations and show stability for the low and intermediate frequencies. Note that this analysis does not provide any information about the highest frequencies and therefore does not prove stability of the scheme. As we shall see in section 6, numerical calculations show that our A^TA-dissipation takes care of any instabilities caused by the highest frequencies in our scheme. We discuss the modified equation technique here because in the multidimensional case, the use of modified equations is the only way to obtain stability information. Such an analysis can be found in [2]. Since in [2] we neglected the truncation error in the normal direction, it is important that the restriction of the approximation to one dimension is completely stable.

Even though extensive numerical experiments with our two-dimensional scheme indicate that it is stable with A^TA-dissipation, we note that there might be other schemes with stable modified equations which are unstable.

We introduce the dependent variable

$$v(x,t) = u(-x,t),$$

assume $x_{min} \to \infty$, $x_{max} \to \infty$, and write (17), (18) as a half-plane problem for the system

$$\begin{pmatrix} v \\ w \end{pmatrix}_{tt} = \begin{pmatrix} 1 & 0 \\ 0 & c^2 \end{pmatrix} \begin{pmatrix} v \\ w \end{pmatrix}_{xx}, \quad 0 \le x < \infty, \quad t \ge 0, \tag{42}$$

with the modified jump conditions

$$v(0,t) + h^2\beta v_{xx}(0,t) = w(0,t) + h^2\beta w_{xx}(0,t), \tag{43}$$

$$v_x(0,t) + h^2\gamma v_{xxx}(0,t) = -c^2\left(w_x(0,t) + h^2\gamma w_{xxx}(0,t)\right). \tag{44}$$

We obtain (43) and (44) from (25) and (26) by adding the leading truncation error term. A simple but tedious calculation shows that

$$\beta = \frac{(1-\alpha)\alpha}{2}, \quad \gamma = \frac{-2 + 6\alpha - 3\alpha^2}{6}.$$

We use mode analysis to discuss stability. The general solutions of type

$$\begin{pmatrix} v(x,t) \\ w(x,t) \end{pmatrix} = e^{st} \begin{pmatrix} \tilde{v}(x,s) \\ \tilde{w}(x,s) \end{pmatrix}, \quad \mathrm{Re}(s) \ge 0,$$

where $(\tilde{v}(x,s), \tilde{w}(x,s))$ are bounded, are given by

$$v(x,t) = e^{st}e^{-sx}v_0, \quad w(x,t) = e^{st}e^{-(s/c)x}w_0. \tag{45}$$

Introducing (45) into the boundary conditions (43), (44) gives us

$$\begin{aligned}(1+h^2\beta s^2)v_0 - (1+h^2\beta s^2)w_0 &= 0,\\ (1+h^2\gamma s^2)v_0 + c^2(1+h^2\gamma s^2)w_0 &= 0.\end{aligned}$$

Thus, nontrivial solutions exist if and only if

$$-(1+h^2\beta s^2)(1+h^2\gamma s^2) = 0.$$

Hence, instabilities can only be present for $s = \mathcal{O}(1/h)$, i.e., for high frequencies. (However, the proof in the previous section shows that this cannot happen.)

4. Solvability of the two-dimensional discrete jump conditions. Let the 2×2 matrix on the left-hand side of (16) be P. The linear system has a unique solution if $\det P \neq 0$. We have

$$\det P = g_0^D(\xi_\Gamma)g_0^N(\xi_I - \xi_\Gamma)/\rho_{II} + g_0^D(\xi_I - \xi_\Gamma)g_0^N(\xi_\Gamma)/\rho_I.$$

The coefficients in the Dirichlet formula (8) are

$$g_0^D(\xi) = \frac{(\xi_I - \xi)(2\xi_I - \xi)}{2\xi_I^2} + \delta, \quad g_I^D(\xi) = \frac{\xi(2\xi_I - \xi)}{\xi_I^2} - 2\delta, \quad g_{II}^D(\xi) = \frac{\xi(\xi - \xi_I)}{2\xi_I^2} + \delta,$$

where $\delta \approx 0.25$ is a constant that removes the small-cell time step restriction while preserving the second order accuracy; see [3]. The coefficients in the Neumann formula (9) are (see [2])

$$g_0^N(\xi) = \frac{3\xi_I - 2\xi}{2\xi_I^2}, \quad g_I^N(\xi) = \frac{2\xi - 2\xi_I}{\xi_I^2}, \quad g_{II}^N(\xi) = \frac{\xi_I - 2\xi}{2\xi_I^2}.$$

Since $0 \leq \xi_\Gamma \leq \xi_I$ and $\delta > 0$,

$$0 < \delta \leq g_0^D \leq 1 + \delta, \quad 0 < \frac{1}{2\xi_I} \leq g_0^N \leq \frac{3}{2\xi_I}.$$

Hence

$$\frac{\delta}{2\xi_I}\left(\frac{1}{\rho_I} + \frac{1}{\rho_{II}}\right) \leq \det P \leq \frac{3(1+\delta)}{2\xi_I}\left(\frac{1}{\rho_I} + \frac{1}{\rho_{II}}\right).$$

For all possible directions of the normal, $h \leq \xi_I \leq \sqrt{2}h$, and we conclude that

$$\det P \geq C > 0, \quad C = \frac{\delta}{2\sqrt{2}h}\left(\frac{1}{\rho_I} + \frac{1}{\rho_{II}}\right).$$

The fact that the lower bound of $\det P$ is proportional to δ shows that the δ-term is essential for the solvability of the discrete jump conditions for general locations of the interface relative to the grid. The δ-term was originally designed for Dirichlet boundary conditions to remove the small-cell time step restriction (cf. [3]), and it also serves that purpose here.

5. Time-integration and A^TA-dissipation. The discretized jump conditions (16) can in principle be used to eliminate all ghost points from the discrete approximation of the Laplacians of u and w (7). Since the jump conditions couple the solutions on both sides of the interface, the matrix form of the discrete Laplacian becomes

$$\begin{aligned} \Delta_h u(\boldsymbol{X}_I, t_n) &= A_{11}\boldsymbol{u}^n + A_{12}\boldsymbol{w}^n, \\ \Delta_h w(\boldsymbol{X}_{II}, t_n) &= A_{21}\boldsymbol{u}^n + A_{22}\boldsymbol{w}^n, \end{aligned} \qquad A = \begin{pmatrix} A_{11} & A_{12} \\ A_{21} & A_{22} \end{pmatrix}.$$

Here, $\boldsymbol{X}_I$ and $\boldsymbol{X}_{II}$ are vectors of all grid point coordinates inside Ω_I and Ω_{II}, respectively, and $\boldsymbol{u}$ and $\boldsymbol{w}$ are the discrete solutions at those grid points. If all eigenvalues of A are distinct, real, and negative, one can show that the scheme

$$\begin{pmatrix} \rho_I(\boldsymbol{u}^{n+1} - 2\boldsymbol{u}^n + \boldsymbol{u}^{n-1})/\delta_t^2 \\ \rho_{II}(\boldsymbol{w}^{n+1} - 2\boldsymbol{w}^n + \boldsymbol{w}^{n-1})/\delta_t^2 \end{pmatrix} = A \begin{pmatrix} \boldsymbol{u}^n \\ \boldsymbol{w}^n \end{pmatrix} + \boldsymbol{F}(t_n) \tag{46}$$

is stable for sufficiently small time steps δ_t [1]. However, the embedded boundary approximation of the jump conditions breaks the symmetry of the matrix A so it is not possible to guarantee this property. In fact, numerical examples (see section 6) indicate that the above scheme suffers from a mild instability.

In the previous embedded boundary methods for the wave equation subject to Neumann [2] and Dirichlet [3] boundary conditions, we damped the instability by adding a small fourth order term of the type $h^3 A^T A(\boldsymbol{u}_t, \boldsymbol{w}_t)^T$ to the right-hand side of (46). While this technique turned out to work very well in practice for the Neumann and Dirichlet problems, it is not directly amendable to the current problem because the matrix A couples the solutions across the interface. Consequently, it becomes complicated to evaluate A^T on a solution vector without explicitly forming the matrix A.

It is not difficult to modify the previous dissipation technique to work with the jump conditions. We first describe the idea for the continuous problem. For the wave equation (1)–(2) with jump conditions (5)–(6), we can evaluate the normal derivative of the solutions on either side of the interface as functions of time,

$$\frac{\partial u}{\partial n}(\boldsymbol{x}, t) =: f_I(\boldsymbol{x}, t), \quad \boldsymbol{x} \in \Gamma,\ t \geq 0, \tag{47}$$

$$\frac{\partial w}{\partial n}(\boldsymbol{x}, t) =: f_{II}(\boldsymbol{x}, t), \quad \boldsymbol{x} \in \Gamma,\ t \geq 0. \tag{48}$$

Hence, once the continuous problem with jump conditions has been solved, we can in principle recompute the same solution by solving two uncoupled Neumann problems:

$$\begin{aligned} \rho_I u_{tt} &= \Delta u + F(\boldsymbol{x}, t), && \boldsymbol{x} \in \Omega_I, && t \geq 0, \\ \frac{\partial u}{\partial n}(\boldsymbol{x}, t) &= f_I(\boldsymbol{x}, t), && \boldsymbol{x} \in \Gamma, && t \geq 0, \\ u(\boldsymbol{x}, 0) = U_0(\boldsymbol{x}), \quad u_t(\boldsymbol{x}, 0) &= U_1(\boldsymbol{x}), && && \boldsymbol{x} \in \Omega_I, \end{aligned} \tag{49}$$

and

$$\begin{aligned} \rho_{II} w_{tt} &= \Delta w + F(\boldsymbol{x}, t), && \boldsymbol{x} \in \Omega_{II}, && t \geq 0, \\ \frac{\partial w}{\partial n}(\boldsymbol{x}, t) &= f_{II}(\boldsymbol{x}, t), && \boldsymbol{x} \in \Gamma, && t \geq 0, \\ w(\boldsymbol{x}, 0) = W_0(\boldsymbol{x}), \quad w_t(\boldsymbol{x}, 0) &= W_1(\boldsymbol{x}), && && \boldsymbol{x} \in \Omega_{II}. \end{aligned} \tag{50}$$

Our basic idea is to use the stabilized embedded boundary scheme for the Neumann problem described in [2], where the forcing functions f_I and f_{II} are computed on the fly during the time evolution.

For conciseness, we describe only the details for the Neumann problem (49), which is discretized on the same Cartesian grid as above, leading to the same set of ghost points G_I where the discrete boundary conditions are applied,

$$B^N_{i,j} u^n = f_I(\boldsymbol{x}^\Gamma_{i,j}, t_n), \quad (i,j) \in G_I. \tag{51}$$

The formula (7) for discretizing the Laplacian of u is the same as before, but since the Neumann problem for u is decoupled from w, we now get the matrix representation

$$\Delta_h u(\boldsymbol{X}_I, t_n) = A_I \boldsymbol{u}^n + \boldsymbol{b}^n_I, \tag{52}$$

after all ghost points have been eliminated from (7). The vector $\boldsymbol{b}_I$ contains the discrete boundary forcing function corresponding to the forcing function $f_I(\boldsymbol{x}^\Gamma, t)$ and is only nonzero at grid points just inside the boundary; see [2] for details.

The stabilized scheme for the Neumann problem is

$$\begin{aligned} \rho_I(\boldsymbol{u}^{n+1} - 2\boldsymbol{u}^n + \boldsymbol{u}^{n-1})/\delta_t^2 &= A_I \boldsymbol{u}^n + \boldsymbol{b}^n + \boldsymbol{F}(t_n) \\ &\quad - \epsilon \frac{h^3}{\delta_t} A_I^T \left(A_I \boldsymbol{u}^n + \boldsymbol{b}^n - A_I \boldsymbol{u}^{n-1} - \boldsymbol{b}^{n-1} \right), \end{aligned} \tag{53}$$

where $\epsilon > 0$ is a small constant. Numerical experiments indicate that $\epsilon = \mathcal{O}(10^{-3})$ is sufficient to allow for very long time-integrations (10^6 time steps or more). The scheme (54) can be recast into an equivalent form that makes it easier to generalize to handle the jump conditions. Let us define an extended solution vector $\bar{\boldsymbol{u}}$ that includes the solution at all interior points as well as the ghost points. Given $\bar{\boldsymbol{u}}$, all values are defined to evaluate the discrete Laplacian $\Delta_h u_{i,j}$ (7) at all points $\boldsymbol{x}_{i,j} \in \Omega_I$. We write the discrete Laplacian at all these points as $\Delta_h \bar{\boldsymbol{u}}$ and arrive at the equivalent method:

1. Given $\boldsymbol{u}^n$, define $\bar{\boldsymbol{u}}^n$ by assigning all ghost points to satisfy the discretized Neumann boundary condition (51).
2. Update all interior points $\boldsymbol{x}_{i,j} \in \Omega_I$ by

$$\begin{aligned} \rho_I(\boldsymbol{u}^{n+1} - 2\boldsymbol{u}^n + \boldsymbol{u}^{n-1})/\delta_t^2 &= \Delta_h \bar{\boldsymbol{u}}^n + \boldsymbol{F}(t_n) \\ &\quad - \epsilon \frac{h^3}{\delta_t} A_I^T \left(\Delta_h \bar{\boldsymbol{u}}^n - \Delta_h \bar{\boldsymbol{u}}^{n-1} \right). \end{aligned} \tag{54}$$

Using this formulation shows that the matrix A_I is only needed to evaluate the dissipation term, and only for the matrix-vector product $A_I^T \boldsymbol{y}$, where $\boldsymbol{y} = \Delta_h \bar{\boldsymbol{u}}^n - \Delta_h \bar{\boldsymbol{u}}^{n-1}$. Note that the boundary forcing $f_I(\boldsymbol{x}^\Gamma, t)$ influences only the ghost point values and has no bearing on A_I^T.

To satisfy the discrete jump conditions (14)–(15), it appears that we must first calculate a corresponding value of f_I to use in (51). Given $\boldsymbol{u}^n$, this can be achieved by first calculating the values at all ghost points G_I by solving the 2×2 linear system (16). We can then use the embedded boundary formula (51) to evaluate f_I. However, it is a trivial exercise to see that enforcing (51) with this f_I results in the same ghost point values as those we started with. Hence, it is not necessary to calculate f_I, and we can simply replace the inhomogeneous Neumann condition by the discrete jump conditions (16). The same principle applies to the Neumann problem in Ω_{II} and we arrive at the damped scheme for the problem with jump conditions:

1. Given $\boldsymbol{u}^n$ and $\boldsymbol{w}^n$, define $\bar{\boldsymbol{u}}^n$ by assigning all ghost points $u_{i,j}$ to satisfy the discrete jump conditions along normals going through $(i,j) \in G_I$,
$$B^D_{i,j} u^n = V^D_{i,j} w^n,$$
$$\frac{1}{\rho_I} B^N_{i,j} u^n = -\frac{1}{\rho_{II}} V^N_{i,j} w^n.$$
2. Given $\boldsymbol{u}^n$ and $\boldsymbol{w}^n$, define $\bar{\boldsymbol{w}}^n$ by assigning all ghost points $w_{i,j}$ to satisfy the discrete jump conditions along normals going through $(i,j) \in G_{II}$,
$$B^D_{i,j} w^n = V^D_{i,j} u^n,$$
$$\frac{1}{\rho_{II}} B^N_{i,j} w^n = -\frac{1}{\rho_I} V^N_{i,j} u^n.$$
3. Update all interior points $\boldsymbol{x}_{i,j} \in \Omega_I$ by
$$\rho_I(\boldsymbol{u}^{n+1} - 2\boldsymbol{u}^n + \boldsymbol{u}^{n-1})/\delta_t^2 = \Delta_h \bar{\boldsymbol{u}}^n + \boldsymbol{F}(t_n) - \epsilon \frac{h^3}{\delta_t} A_I^T \left(\Delta_h \bar{\boldsymbol{u}}^n - \Delta_h \bar{\boldsymbol{u}}^{n-1}\right).$$
4. Update all interior points $\boldsymbol{x}_{i,j} \in \Omega_{II}$ by
$$\rho_{II}(\boldsymbol{w}^{n+1} - 2\boldsymbol{w}^n + \boldsymbol{w}^{n-1})/\delta_t^2 = \Delta_h \bar{\boldsymbol{w}}^n + \boldsymbol{F}(t_n) - \epsilon \frac{h^3}{\delta_t} A_{II}^T \left(\Delta_h \bar{\boldsymbol{w}}^n - \Delta_h \bar{\boldsymbol{w}}^{n-1}\right).$$

Here, A_{II} denotes the matrix representation of the discrete Laplacian subject to discrete Neumann conditions in Ω_{II}, and $\bar{\boldsymbol{w}}^n$ is the extended solution vector holding the solution at all interior grid points of Ω_{II} as well as at the ghost points G_{II}. Note that the matrices A_I and A_{II} do not need to be formed explicitly; cf. [2].

The wave equation subject to jump condition is equivalent to the two uncoupled wave equations subject to Neumann boundary conditions (49)–(50), and the theory in [2] shows that the $h^3 A^T A u_t$-dissipation term inflicts an error which is $\mathcal{O}(h^2)$ for these problems. Hence, we conclude that the dissipation term also inflicts an $\mathcal{O}(h^2)$ error for the wave equation with jump conditions.

6. Numerical examples. To test the accuracy of the numerical scheme, we begin by considering electromagnetic scattering of a plane incident wave by a dielectric circular cylinder of radius R. In this section, we follow the notation of electromagnetics and let $\kappa_e \geq 1$ denote the relative permittivity of the dielectric material but assume the same permeability inside and outside the dielectric. By assuming TE_z polarization and scaling time to obtain unit speed of light in vacuum, we arrive at the following problem for the z-component of the magnetic field:

$$\frac{\partial^2 H^{(z)}}{\partial t^2} = \Delta H^{(z)}, \qquad R^2 < x^2 + y^2 < \infty, \tag{55}$$

$$\frac{\partial^2 H^{(z)}}{\partial t^2} = \frac{1}{\kappa_e} \Delta H^{(z)}, \qquad x^2 + y^2 < R^2, \tag{56}$$

subject to the jump conditions

$$\left[H^{(z)}\right] = 0, \quad \left[\frac{1}{\kappa_e} \frac{\partial H^{(z)}}{\partial n}\right] = 0, \quad x^2 + y^2 = R^2.$$

Here, $\partial/\partial n$ denotes the normal derivative on the boundary of the dielectric cylinder and $\kappa_e = 1$ outside the cylinder. There is an analytical solution of this problem due

TABLE 1

Max error at time $T = 10.0$ for the case $\kappa_e = 2$ inside the dielectric cylinder (u_{err}) and outside of it (w_{err}), with A^TA-dissipation ($\epsilon = 10^{-3}$) and without dissipation.

N	h	u_{err}	u_{err}, A^TA	w_{err}	w_{err}, A^TA
201	1.5×10^{-2}	4.50×10^{-2}	4.47×10^{-2}	2.07×10^{-2}	2.09×10^{-2}
401	7.5×10^{-3}	1.12×10^{-2}	1.11×10^{-2}	5.44×10^{-3}	5.49×10^{-3}
801	3.75×10^{-3}	2.81×10^{-3}	2.80×10^{-3}	1.30×10^{-3}	1.31×10^{-3}

TABLE 2

Max error at time $T = 200.0$ for the case $\kappa_e = 2$ inside the dielectric cylinder (u_{err}) and outside of it (w_{err}). The coefficient in the A^TA-dissipation was $\epsilon = 10^{-3}$.

N	h	Time steps	u_{err}, A^TA	w_{err}, A^TA
201	1.5×10^{-2}	26,666	3.38×10^{-2}	3.57×10^{-2}
401	7.5×10^{-3}	53,333	8.42×10^{-3}	7.82×10^{-3}
801	3.75×10^{-3}	106,666	2.31×10^{-3}	1.97×10^{-3}

to Mie (see, for example, [28, p. 667]). Let the incident wave have angular frequency ω and wave number k:

$$H_I^{(z)}(x, y, t) = e^{i(kx-\omega t)}.$$

In polar coordinates (ρ, θ), the incident, scattered, and transmitted fields are

$$H_I^{(z)} = e^{i\omega t} \sum_{n=-\infty}^{\infty} i^{-n} J_n(k\rho) e^{in\theta}, \qquad \rho > R, \tag{57}$$

$$H_S^{(z)} = e^{i\omega t} \sum_{n=-\infty}^{\infty} i^{-n} a_n H_n^{(2)}(k\rho) e^{in\theta}, \quad \rho > R, \tag{58}$$

$$H_D^{(z)} = e^{i\omega t} \sum_{n=-\infty}^{\infty} i^{-n} b_n J_n(mk\rho) e^{in\theta}, \quad \rho < R, \tag{59}$$

where $m = \sqrt{\kappa_e}$, J_n is the Bessel function of the first kind of order n, and $H^{(2)}$ is the Hankel function of the second kind of order n (corresponding to waves propagating outward). The coefficients a_n and b_n are given in [28, p. 667].

The scattering problem was solved numerically for the case $R = 1$, $\kappa_e = 2$, $\omega = k = 2\pi$. The computational domain was the square $-1.5 \le x \le 1.5$, $-1.5 \le y \le 1.5$, and the exact solution was imposed as a Dirichlet boundary condition on the outer boundary. The exact solution was also imposed as initial condition. The error in the numerical solution measured in max norm over all internal grid points was evaluated at times $T = 10.0$ and $T = 200.0$; see Tables 1 and 2, respectively. Note that the error is second order accurate at both times and of the same order of magnitude for the same grid sizes. Studying the error as function of time (see Figure 5) reveals that the A^TA-dissipation is only necessary for long-time computations. Furthermore, there is no noticable growth of the error after long times when the dissipation is used, indicating that the damping is very weak.

As a second test, we consider the same geometry as above but reduce the wave speed inside the cylinder by setting $\kappa_e = 10$. Hence the wave length inside the cylinder

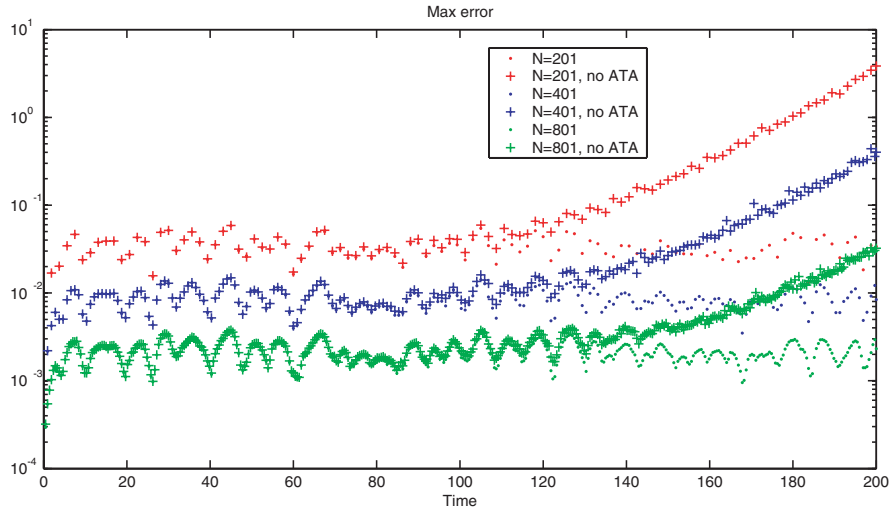

FIG. 5. *The max error inside the dielectric cylinder (u_{err}) as function of time for the case $\kappa_e = 2$, for different grid sizes, with and without A^TA-dissipation.*

TABLE 3

Max error at time $T = 10.0$ for the case $\kappa_e = 10$ inside the dielectric cylinder (u_{err}) and outside of it (w_{err}), with A^TA-dissipation ($\epsilon = 10^{-3}$) and without dissipation.

N	h	u_{err}	u_{err}, A^TA	w_{err}	w_{err}, A^TA
401	7.5×10^{-3}	2.17×10^{-1}	2.16×10^{-1}	6.52×10^{-2}	6.48×10^{-2}
801	3.75×10^{-3}	5.48×10^{-2}	5.47×10^{-2}	1.62×10^{-2}	1.61×10^{-2}

will be a factor $\sqrt{10}$ smaller than outside of it. For this reason, a smaller grid size is needed to resolve the solution and the grid with $N = 201$ is no longer adequate. The errors in the solution at times $T = 10$ and $T = 200$ are given in Tables 3 and 4, respectively. Even though the errors are larger in this case, they are still second order accurate at both times and of the same order of magnitude for the same grid sizes. The solution at time $T = 10$ is shown in Figure 6.

To illustrate that the method generalizes to many subdomains, we consider the scattering of a plane incoming wave on a media with different wave speeds inside each bubble; see Figure 7. This calculation was started from homogeneous initial data and driven on the left boundary by the data $u(-2, y, t) = \sin(8\pi t)$. The remaining outer boundaries had homogeneous Neumann conditions. The solution is shown at time $T = 5$. The ambient media has unit wave speed, so this time corresponds closely to the first arrival of the solution at the right boundary. Note that the speed inside the top bubble (which breaks the otherwise symmetrical configuration) equals the unit speed in the ambient media, but the jump conditions are enforced across its interface. Nevertheless, the contour lines of the numerical solution display a high degree of symmetry about the $y = 0$ axis, indicating that the truncation errors in the jump conditions are very small.

To further illustrate the flexibility of the method, we calculate the scattering around an irregular shape described by a periodic cubic spline curve; see Figure 8. Note that the interface has both concave and convex parts. The wave speed inside

TABLE 4

Max error at time $T = 200.0$ for the case $\kappa_e = 10$ inside the dielectric cylinder (u_{err}) and outside of it (w_{err}). The coefficient in the A^TA-dissipation was $\epsilon = 10^{-3}$.

N	h	Time steps	u_{err}, A^TA	w_{err}, A^TA
401	7.5×10^{-3}	53,333	2.03×10^{-1}	7.16×10^{-2}
801	3.75×10^{-3}	106,666	5.81×10^{-2}	1.75×10^{-2}

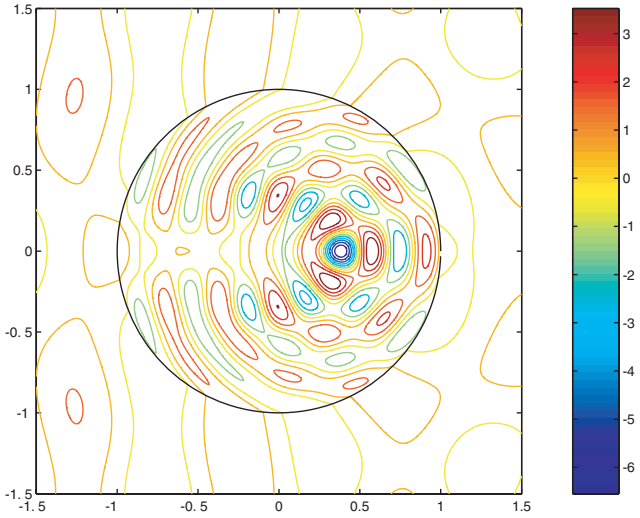

FIG. 6. *The Mie scattering solution at time $T = 10$ with $\kappa_e = 10$. Note the focusing of the wave inside the cylinder.*

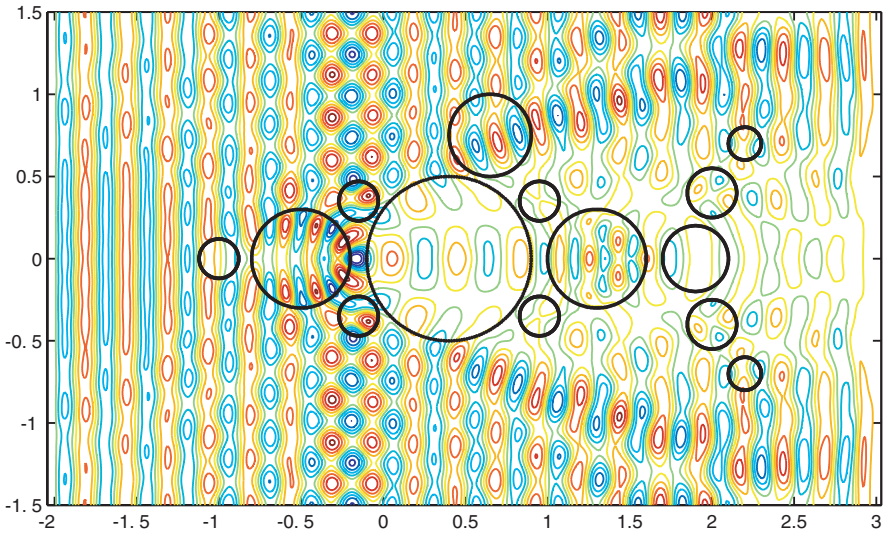

FIG. 7. *An incoming planar wave scattered by several bubbles with both larger and smaller wave speed compared to the ambient media.*

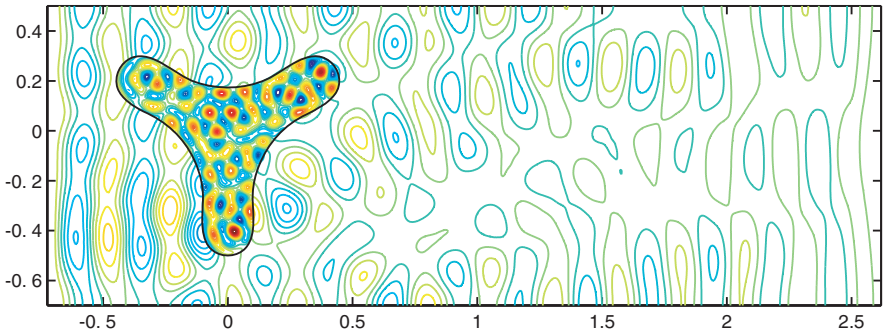

FIG. 8. *An incoming planar wave scattered by an irregular shape described by a periodic spline curve. The wave speed inside the curve was a factor* $\sqrt{10}$ *smaller than on the outside.*

the shape was $1/\sqrt{10}$ and the ambient wave speed was one. As in the previous example, the calculation was started from homogeneous initial conditions and driven on the left boundary by the data $u(-0.7, y, t) = \sin(8\pi t)$. Homogeneous Neumann conditions were imposed on the remaining boundaries. The solution is shown at time $T = 3.3$, which approximately corresponds to when the initial wave front reaches the right boundary.

7. Conclusions. We have developed a second order accurate embedded boundary method for the two-dimensional wave equation with discontinuous coefficients. The current method uses the same grid size throughout the computational domain, but as the jump in wave speed across the interface gets larger, it becomes obvious that this approach either overresolves the solution on one side of the interface or underresolves it on the other side. It would therefore be desirable to extend the method to handle different mesh sizes on different sides of the interface; some initial steps have been taken in this direction. We also expect to generalize the method to handle the more complicated jump conditions associated with the elastic wave equation with discontinuous coefficients.

REFERENCES

[1] H.-O. KREISS, N. A. PETERSSON, AND J. YSTRÖM, *Difference approximations for the second order wave equation*, SIAM J. Numer. Anal., 40 (2002), pp. 1940–1967.

[2] H.-O. KREISS, N. A. PETERSSON, AND J. YSTRÖM, *Difference approximations of the Neumann problem for the second order wave equation*, SIAM J. Numer. Anal., 42 (2004), pp. 1292–1323.

[3] H.-O. KREISS AND N. A. PETERSSON, *A second order accurate embedded boundary method for the wave equation with Dirichlet data*, SIAM J. Sci. Comput., 27 (2006), pp. 1141–1167.

[4] R. B. PEMBER, J. B. BELL, P. COLLELLA, W. Y. CRUTCHFIELD, AND M. WELCOME, *An adaptive Cartesian grid method for unsteady compressible flow in irregular regions*, J. Comput. Phys., 120 (1995), pp. 278–304.

[5] M. J. BERGER, C. HELZEL, AND R. J. LEVEQUE, *h-Box methods for the approximation of hyperbolic conservation laws on irregular grids*, SIAM J. Numer. Anal., 41 (2003), pp. 893–918.

[6] A. DITKOWSKI, K. DRIDI, AND J. S. HESTHAVEN, *Convergent Cartesian grid methods for Maxwell's equations in complex geometries*, J. Comput. Phys., 170 (2001), pp. 39–80.

[7] B. GUSTAFSSON, H.-O. KREISS, AND J. OLIGER, *Time Dependent Problems and Difference Methods*, Wiley–Interscience, New York, 1995.

[8] G. BROWNING, H-.O. KREISS, AND J. OLIGER, *Mesh refinement*, Math. Comp., 27 (1973), pp. 29–39.

[9] D. L. Brown, *A note on the numerical solution of the wave equation with piecewise smooth coefficients*, Math. Comput., 42 (1984), pp. 369–391.
[10] A. N. Tikhonov and A. A. Samarskiĭ, *Homogeneous difference schemes*, Zh. Vychisl. Mat. i Mat. Fiz., 1 (1961), pp. 5–63.
[11] C. Zhang and R. LeVeque, *The immersed interface method for acoustic wave equations with discontinuous coefficients*, Wave Motion, 25 (1997), pp. 237–263.
[12] J. S. Hesthaven, *High-order accurate methods in time-domain computational electromagnetics*, Advances in Imaging and Electron Physics, 127 (2003), pp. 59–123.
[13] S. Zhao and G. W. Wei, *High-order FDTD methods via derivative matching for Maxwell's equations with material interfaces*, J. Comput. Phys., 200 (2004), pp. 60–103.
[14] A. Yefet and E. Turkel, *Fourth order compact implicit method for the Maxwell equations with discontinuous coefficients*, Appl. Numer. Math., 33 (2000), pp. 125–134.
[15] A. Yefet and P. G. Petropoulos, *A staggered fourth-order accurate explicit finite difference scheme for the time-domain Maxwell's equations*, J. Comput. Phys., 168 (2001), pp. 286–315.
[16] Z. Xie, C.-H. Chan, and B. Zhang, *An explicit fourth-order staggered finite-difference time-domain method for Maxwell's equations*, J. Comput. Appl. Math., 147 (2002), pp. 75–98.
[17] E. Turkel and A. Yefet, *On the construction of a high order difference scheme for complex domains in a Cartesian grid*, Appl. Numer. Math., 33 (2000), pp. 113–124.
[18] W. Cai and S. Z. Deng, *An upwinding embedded boundary method for Maxwell's equations in media with material interfaces: 2D case*, J. Comput. Phys., 190 (2003), pp. 159–183.
[19] Z. Xie, C.-H. Chan, and B. Zhang, *An explicit fourth-order curvilinear staggered-grid FDTD method for Maxwell's equations*, J. Comput. Phys., 175 (2002), pp. 739–763.
[20] T. A. Driscoll and B. Fornberg, *Block pseudospectral methods for Maxwell's equations* II: *Two-dimensional, discontinuous-coefficient case*, SIAM J. Sci. Comput., 21 (1999), pp. 1146–1167.
[21] R. Weller and G. H. Shortley, *Calculation of stresses within the boundary of photoelastic models*, J. Appl. Mech., 6 (1939), pp. A71–A78.
[22] H. Johansen and P. Colella, *A Cartesian grid embedded boundary method for Poisson's equation on irregular domains*, J. Comput. Phys., 147 (1998), pp. 60–85.
[23] P. A. Berthelsen, *A decomposed immersed interface method for variable coefficient elliptic equations with nonsmooth and discontinuous solutions*, J. Comput. Phys., 197 (2004), pp. 364–386.
[24] A. L. Fogelson and J. P. Keener, *Immersed interface methods for Neumann and related problems in two and three dimensions*, SIAM J. Sci. Comput., 22 (2000), pp. 1630–1654.
[25] Z. Li and K. Ito, *Maximum principle preserving schemes for interface problems with discontinuous coefficients*, SIAM J. Sci. Comput., 23 (2001), pp. 339–361.
[26] A. Wiegmann and K. P. Bube, *The immersed interface method for nonlinear differential equations with discontinuous coefficients and singular sources*, SIAM J. Numer. Anal., 35 (1998), pp. 177–200.
[27] G. Mie, *Beiträge zur optik trüber medien, speziell kolloidaler metallösungen*, Annalen der Physik, 25 (1908), pp. 377–445.
[28] C. A. Balanis, *Advanced Engineering Electromagnetics*, Wiley, New York, 1989.